Japanese Journal of Applied Physics
Vol. 44, No. 7B, 2005, pp. 5443–5446

Observation of Large-Scale Features on Graphite by Scanning Tunnelling Microscopy

Wing-Tat PONG, James BENDALL and Colm DURKAN*

Nanoscience Centre, University of Cambridge, 11. J J Thomson Ave, Cambridge, CB3 0FF, UK

(Received January 24, 2005; accepted March 16, 2005; published July 26, 2005)

Superlattice structures and rippling fringes were imaged on two separate pieces of graphite (HOPG) by scanning tunnelling microscopy (STM). We observed the corrugation conservation phenomenon on one of the superlattice structures where an overlayer does not attenuate the corrugation amplitude of the superlattice. Such a phenomenon may illustrate an implication that nanoscale defects a few layers underneath the surface may propagate through many layers without decay and form the superlattice structure on the topmost surface. Some rippling fringes with periodicities of 20 nm and 30 nm and corrugations of 0.1 nm and 0.15 nm were observed in the superlattice area and in nearby regions. Such fringes are believed to be due to physical buckling of the surface. The stress required to generate such structures is estimated, and a possible cause is discussed. An equation relating the attenuation factor to the number of overlayers is proposed. [DOI: 10.1143/JJAP.44.5443]

KEYWORDS: graphite, scanning tunnelling microscope, superlattice, rippling fringes, attenuation factor, corrugation conservation, Moiré rotation pattern

1. Introduction

Graphite is one of the most commonly used substrates for scanning probe microscopy experiments because of its chemical inertness, commercial availability, and atomically flat terraces, as well as being easy to cleave to provide a fresh surface. However, it has been reported that graphite has various kinds of defects on its surface,[1,2] and one has to be careful in distinguishing those defects from the features of the deposited materials. Therefore it is of paramount importance to have a detailed understanding of the surface features of graphite.

Amongst the intrinsic defects of graphite, a superperiodic structure named a superlattice has been reported by many groups.[3–9] A superlattice is a lattice structure of hexagonal shape with triangular symmetry, its periodicity is usually several to tens of nanometers and its corrugation is around several angstroms to a nanometer. An explanation as to the origin of such superlattices is the Moiré rotation pattern assumption which states that a superlattice is the consequence of the relative rotation between adjacent graphite layers. The rotation angle θ can be related to the periodicity P by eq. (1)

$$P = \frac{d}{2\sin(\theta/2)}, \tag{1}$$

where d is the atomic lattice constant. By measuring the periodicity of the superlattice from STM images, its corresponding rotation angle can be obtained. Kobayashi[10] has proposed a three-dimensional tunnelling theory to describe superlattices. Moreover, he has suggested that nanoscale features are visible even if they are buried a few layers deep as nanoscale waves may propagate through many layers without decay. This implies that the corrugation amplitude of a superlattice may not be attenuated by the overlayers in some circumstances. In this work we report the observation of the corrugation conservation phenomenon in which the corrugation amplitude is conserved even with an overlayer, and also the case where the overlayer attenuates the superlattice corrugation.

Our observed rippling fringes are some fringe structures with periodicities of around 20 nm and 30 nm and corrugations of around 0.1 nm and 0.15 nm. The fringes occur in one of the superlattice regions and the area nearby, and they extend over a few hundred nanometers. These fringe distortions seem to indicate a physical deformation which extends and contracts the layer simultaneously. In this paper, a simple calculation is performed to estimate the magnitude of stress required to generate those rippling fringes, and a possible origin of those fringes is suggested in order to provide an overall picture of the graphite surface condition.

2. Experiment

Experiments were performed on two pieces of highly oriented pyrolytic graphite (HOPG). The samples were cleaved by adhesive tape for a few times before scanning. A home-made STM[11] and a Nanosurf STM[12] were operated in constant-current mode to carry out the experiments under ambient conditions. Mechanically cut Pt/Ir tips were used for imaging.

3. Results and Discussion

The first image in Fig. 1(a) shows a superlattice structure extending across a monoatomic step edge and covering an area of around 200 nm × 200 nm. The superlattice has

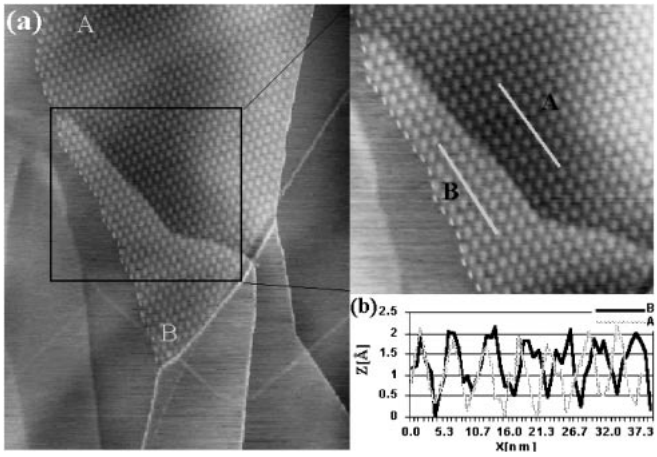

Fig. 1. (a) 319 nm × 300 nm image ($I_t = 0.5$ nA, $V_t = 230$ mV) on graphite with the superlattice structure covering about 200 nm^2 area. The zoom-in on the right shows the superlattice in region A and B more clearly. The superlattice extends across the monoatomic step edge without much attenuation as we can observe in the cross-section in Fig. 1(b). Figure 1(b) shows the cross-sections in region A and B.

*Corresponding author. E-mail address: cd229@eng.cam.ac.uk

boundaries on the left and right, and the step edge at the middle separates the superlattice into two areas which are labelled region A and region B in the figure. Figure 1(b) shows the cross-sections of both regions. As we can see from the cross-sections, the corrugations in region A and B are more or less the same. However, it is reported in the literature[4,5] that the corrugation of a superlattice stretching across a monoatomic step edge will be attenuated by the overlayer by a factor of around 2. In our case, there is no detectable attenuation in corrugations from region A into region B. This corrugation conservation phenomenon may exhibit an implication that nanoscale features can propagate through many layers without decay and form the superlattice on the surface.

The superlattice on another piece of graphite is displayed in Fig. 2(a). Due to the lack of contrast, we cannot see many features apart from the superlattice itself from the image. The contrast of the image is enhanced by changing the colour scheme, and it is displayed in 3-dimensional form in Fig. 2(b). From Fig. 2(b), we can observe rippling fringes at the corner (Fringe A) and in the centre (Fringe B). Figures 2(c) and 2(d) are the line profiles of Fringe A and B respectively. Fringe A has a periodicity of around 20 nm with corrugation of about 0.1 nm while the periodicity and corrugation of Fringe B are around 30 nm and 0.15 nm respectively. Fringe A was imaged under two different tunnelling conditions, and the fringe structure can be observed in both Figs. 2(c) and 2(e). Moreover, the electronic wavelength on a planar graphite sheet is calculated to be 2.51 nm from eq. (2)

$$\lambda = \frac{h}{m_e v_f}, \tag{2}$$

where h is the Planck's constant, m_e is the electron mass, and v_f is the Fermi velocity on planar graphite; from the gradient of the energy-band structure of a graphite sheet at the Fermi surface, we find that the Fermi velocity is $2.9 \times 10^5\,\mathrm{ms}^{-1}$. The electronic wavelength is smaller than those periodicities of Fringe A and B by an order of magnitude, and therefore those fringes are unlikely to be an electronic standing wave on the surface. The fact that the fringe structures were observed under different tunnelling conditions and they are not an electronic wave inclines us to think that those rippling fringes are related to the actual surface topography of graphite, and they are not just an electronic effect. Some rippling fringes were imaged in the nearby regions as well. Similar fringes can be observed in the central part of Fig. 3(b) which is a 3-dimensional image of Fig. 3(a) with enhanced contrast. In addition, to the bottom left corner of Figs. 3(b) and 3(a), there is a pit of monolayer depth associated with some rippling fringes [see Fig. 3(c)] which stretch from the pit, along around 700 nm, to the step edge at the upper part of the image. Rippling fringes were observed across a number of different areas and were not confined to one particular region.

A simple model is established for these rippling fringes, and an estimation of the stress required to generate those fringes is made. A graphite layer under zero applied force

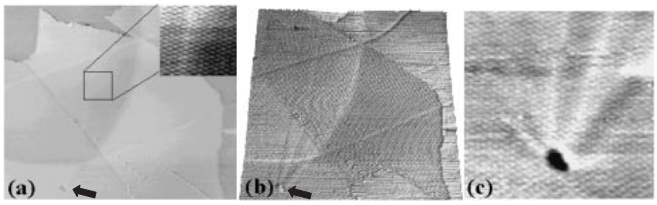

Fig. 3. Another area with rippling fringes. (a) 800 nm × 750 nm image ($I_t = 0.5$ nA, $V_s = 206$ mV) with most of the area being superlattice as shown by the inset. (b) The 3D and contrast-enhanced image of Fig. 3(a), from where we can observe the rippling fringes again localized in the central part of the image. (c) The pit of monolayer deep associated with some long-ranged fringes which is positioned at the bottom left hand corner of Figs. 3(a) and 3(b) indicated by the arrows.

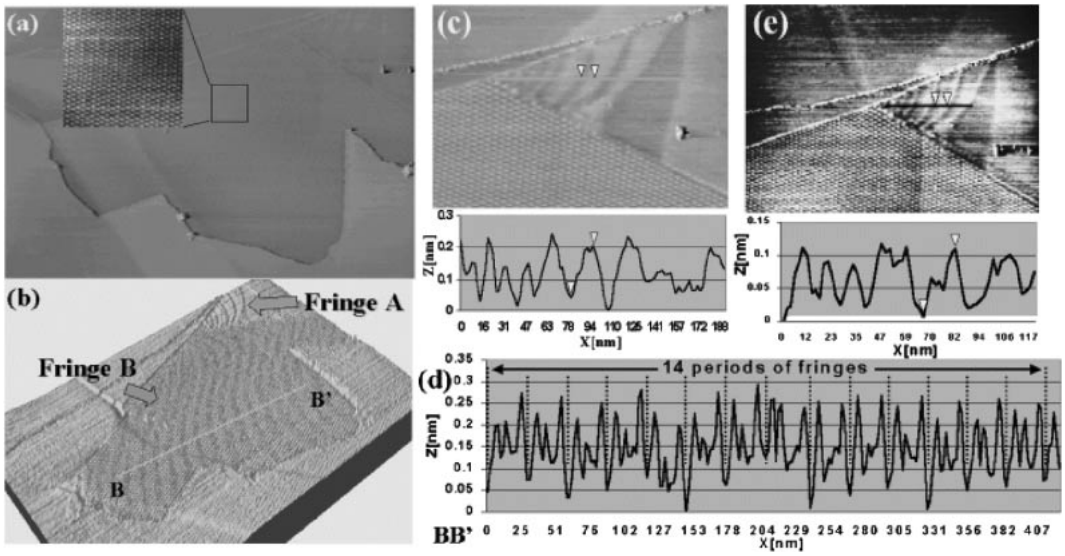

Fig. 2. The rippling fringes on the graphite. (a) 700 nm × 500 nm image ($I_t = 0.36$ nA, $V_s = 450$ mV) on graphite with the central part being the superlattice as shown by the inset. (b) 3D image of Fig. 2(a) with the contrast enhanced. The fringes at the corner and in the central part are labeled as Fringe A and Fringe B respectively. The line profile BB′ is shown in Fig. 2(d). (c) 290 nm × 200 nm image ($I_t = 0.5$ nA, $V_s = 206$ mV) of Fringe A in Fig. 2(b) with its cross-section. (d) Cross-section of Fringe B along BB′ in Fig. 2(b). There are 14 periodicities of the rippling fringes shown in Fig. 2(b). The fringes are buried in the superlattice, so the contrast has to be enhanced in order to display the rippling fringes in Fig. 2(b). (e) 400 nm × 350 nm image ($I_t = 0.36$ nA, $V_s = 450$ mV) of Fringe A in Fig. 2(b) with its cross-section.

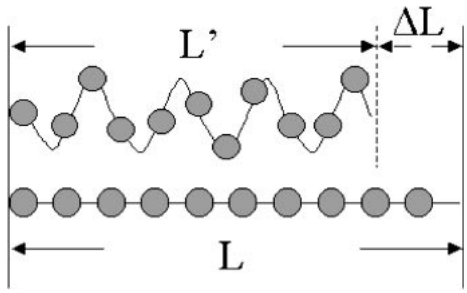

Fig. 4. When there is no applied force, the graphite layer is flat and its length is L. As force is applied, the layer becomes buckled and its horizontal length decreases by ΔL and becomes L'.

will be flat and has a corresponding length, L. When a lateral force is applied to the layer, it buckles and the atomic spacing becomes smaller in order to provide resistive force to act against and balance the applied force. Its horizontal length decreases by ΔL to L' (Fig. 4). When the surface is buckled, since the atomic spacing is now smaller, the Young's modulus will be larger. However, we do not know how much smaller the atomic spacing becomes and thus do not know the actual Young's modulus. In this case, we can only use the normal Young's modulus of graphite for calculation. The surface buckling is modelled as a sinusoidal wave, and the normal Young's modulus of graphite, E ($121.9 \times 10^9\,\mathrm{Nm^{-2}}$), is obtained from ref. 13. Using $L' = 400\,\mathrm{nm}$ which is approximately the length of the rippling region of Fringe B and working through eqs. (3)–(5), the stress is found to be 170 MPa which is a lower bound value for the actual stress because the Young's modulus used in this calculation is smaller than the actual one.

$$\Delta L = L - L' \tag{3}$$

$$L = \int_0^{L'} \sqrt{1 + (A/2)^2 \cos^2(2\pi \frac{x}{T})}\mathrm{d}x \tag{4}$$

$$E = stress/strain \tag{5}$$

where A is the corrugation amplitude (0.15 nm) and T is the periodicity of fringe (30 nm).

Simulations of the superlattice based on the assumption of Moiré rotation pattern were performed and rippling fringes were not observed in the simulation results. This confirms our experimental finding that those rippling fringes are not related to the superlattice itself and their formation is due to something else. Details of the simulation can be found in ref. 14. Analysis on Fig. 3(b) may give us some hints about the possible cause of the rippling fringes. Figure 5 is about the same area as in Fig. 3(b) but with the image divided into domains. From Table I, we can observe that there is quite a wide range of values for periodicities of the superlattices in the image of Fig. 5. However, if we focus within each domain, the variation is actually not too broad, and therefore a representative periodicity is selected for each domain. According to the Moiré rotation pattern assumption, the change of a superlattice periodicity is related to the change of a rotation angle. The fact that the periodicity is changing from one domain to another, especially among domains E–K, means that each domain has a different rotation angle and thus the domains are rotating against each other. In this way, a lot of intralayer stress is generated, and we think it is the possible cause of the physical buckling of the surface which appeared as those rippling fringes under the STM.

The superlattice in Fig. 6 extends across a monoatomic step, and this time the overlayer attenuates the superlattice corrugation with the attenuation factor (AF) of 2.3. Liu *et al.* has reported an AF of 5 for two overlayers.[9] Putting this data into eq. (6), which we propose for relating an AF_n to its corresponding number of overlayers n, we can work out K_1 to be 1 and K_2, which we name the "attenuation coefficient", to be 0.81.

$$AF_n = K_1 \mathrm{e}^{K_2 n} \tag{6}$$

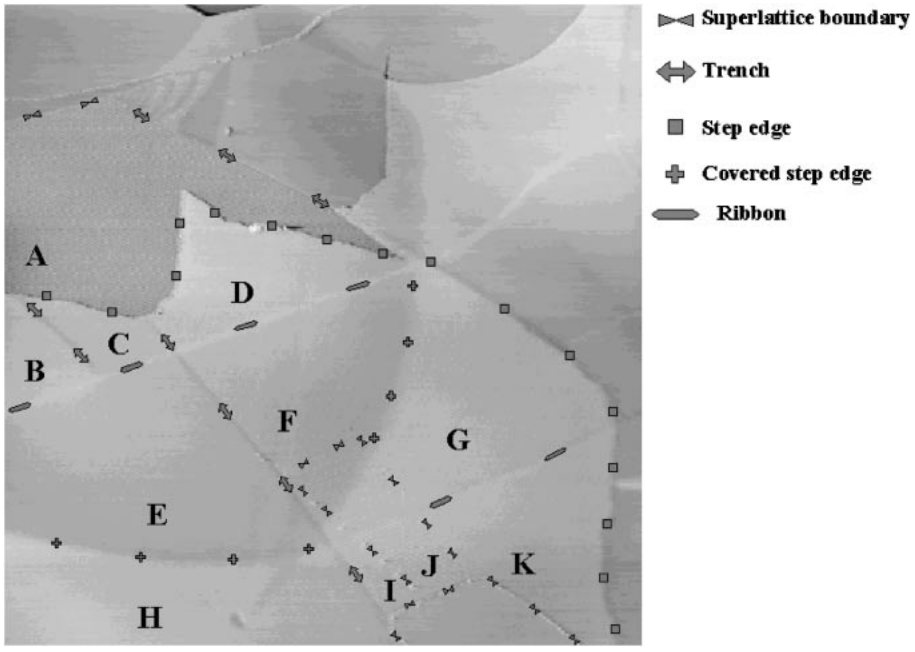

Fig. 5. 1000 nm × 1000 nm ($I_t = 0.5$ nA, $V_s = 206$ mV) image which is about the same area as in Figs. 3(a) and 3(b). Different kinds of superlattice domain boundaries are marked with different labels.

Table I. The periodicities and rotation angle for each domain shown in Fig. 5.

Domain	Periodicities within domain (Å)	Representative periodicity for each domain (Å)	Representative rotation angle for each domain (deg)
A	49.8, 50.3, 50.8, 48.7, 50.5, 48.3, 5.09, 51.4, 50.3	50 ± 2	2.82
B	53.5, 54.3	54 ± 1	2.61
C	53.9, 54.6, 54.2	54 ± 1	2.61
D	52.9, 51.5, 52.1	52 ± 1	2.71
E	57.7, 57.5, 55.1, 57.1, 57.8	57 ± 2	2.47
F	56.2, 56.2, 53.0, 55.0, 55.2	54 ± 2	2.61
G	52.6, 54.8, 54.2, 54.2, 55.8	54 ± 2	2.61
H	63.3, 63.1, 65.3, 66.6, 64.9	65 ± 2	2.17
I	63.3, 64.8	63 ± 1	2.24
J	62.0, 66.3, 72.1, 76.8	70 ± 8	2.01
K	58.1, 58.0, 59.1, 60.4	59 ± 1	2.39

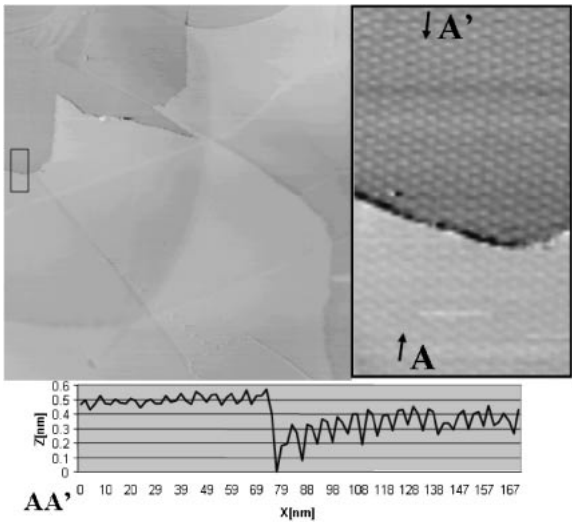

Fig. 6. 935 nm × 853 nm image ($I_t = 0.5$ nA, $V_s = 206$ mV) which is about the same area as in Fig. 3(a). The black squared area on the left is zoomed in and displayed on the right where we can observe a superlattice being attenuated by an overlayer. The cross-section along AA′ is shown at the bottom.

This equation predicts the AF_3 for three overlayers to be 11.4. The attenuation of the corrugation of this superlattice is in stark contrast to the corrugation conservation observed in Fig. 1(a). The superlattice in Fig. 6 is due to the Moiré rotation pattern and thus shows attenuation in the presence of overlayers. The superlattice in Fig. 1(a) is more complex to understand, as within our measurement limits, the corrugation amplitude is identical on both sides of the atomic step. According to our eq. (6), the ratio of the amplitudes of the corrugation on both sides of the step should be $\exp(K_2)$. To fit our data in this case then, K_2 would have to be extremely small, of the order 0.03 or less. This is obviously significantly smaller than the value we have just found of 0.81. We can only speculate that this discrepancy suggests that in this particular case, the superlattice is not entirely due to a Moiré rotation, but may in fact be due to a network of nanoscale defects below the surface.

4. Conclusion

The corrugation conservation phenomenon was observed on a graphite superlattice and this may exhibit an implication that nanoscale defects a few layers underneath the surface propagating through many layers without decay can also be the cause of a superlattice. Some rippling fringes were imaged on the superlattice areas and nearby regions, whose cause may be due to the physical buckling of the surface under intralayer stress, appearing as rippling fringes under the STM. The intralayer stress is explained in terms of different periodicities and thus different rotation angles of the superlattice domains. An equation is proposed to relate the attenuation factor to the number of overlayers, and it predicts the attenuation factor for three overlayers to be 11.4.

Acknowledgment

The authors are grateful for the research fundings by European Union IST project "QIDPPF–ROSES". We would also like to thank Ben Hope, Jize Yan, Hua Ye for valuable discussion.

1) C. R. Clemmer and T. P. Beebe Jr.: Science **251** (1991) 640.
2) H. Chang and A. J. Bard: Langmuir **7** (1991) 1143.
3) Z. Y. Rong and P. Kuiper: Phys. Rev. B **48** (1993) 17427.
4) Z. Y. Rong: Phys. Rev. B **50** (1994) 1839.
5) H. Sun, Q. Shen, J. Jia, Q. Zhang and Q. Xue: Surf. Sci. **542** (2003) 94.
6) M. Kuwabara, D. R. Clarke and D. A. Smith: Appl. Phys. Lett. **56** (1990) 2396.
7) P. I. Oden, T. Thundat, L. A. Nagahara, S. M. Lindsay, G. B. Adams and O. F. Stanley: Surf. Sci. Lett. **254** (1991) L454.
8) J. Xhie, K. Sattler, M. Ge and N. Venkateswaran: Phys. Rev. B **47** (1993) 15835.
9) C. Y. Liu, H. Chang and A. J. Bard: Langmuir **7** (1991) 1138.
10) K. Kobayashi: Phys. Rev. B **53** (1996) 11091.
11) W. T. Pong and C. Durkan: to be published in *Proceedings of the 5th International Conference 7th Annual General Meeting of the European Society for Precision Engineering and Nanotechnology*, Montpellier, France, 2005.
12) easyScan system by Nanosurf AG, Switzerland.
13) T. M. Bernhardt, B. Kaiser and K. Rademann: Surf. Sci. **408** (1998) 86.
14) W. T. Pong and C. Durkan: to be published in Jpn. J. Appl. Phys.